Robust Frequency Control for Varying Inertia Power Systems

George S. Misyris, *Student Member, IEEE,* Spyros Chatzivasileiadis, *Senior Member, IEEE,* and Tilman Weckesser, *Member, IEEE,*

***Abstract*—Increased penetration of fluctuating Renewable Energy Sources (RES) adds a significant uncertainty in the dynamic behavior of the power system. Varying power infeed from RES significantly affects the number of conventional generators to be dispatched at any time instant. As a result, system parameters, such as inertia and damping can no longer be considered constants, but instead they obtain a time-varying profile. In this paper, a robust frequency control scheme is introduced to account for the time-varying system inertia and damping under increased RES penetration. The proposed method is based on an H_∞ loop-shaping design procedure, and it guarantees good frequency response for varying levels of inertia and damping. After presenting the impact of varying system parameters to the system dynamic behavior, the design method for the proposed controller is presented, and its performance in case studies is demonstrated.**

***Index Terms*—frequency dynamics analysis, H_∞ loop-shaping design, robust control.**

I. Introduction

Increased penetration from Renewable Energy Sources (RES) impacts the dynamic behavior of the power system and may jeopardize its stability. In the absence of conventional generators, the Rate Of Change Of Frequency (ROCOF) becomes higher due to the lower inertia, while the frequency nadir deteriorates [1]. Furthermore, conventional generators can assist towards the damping of electromechanical oscillations, and can provide services such as automatic voltage regulation and frequency control [2]. Consequently, transmission system operators face increasing challenges to maintain the security and stability of the electricity network [3].

Generally, RESs do not inherently contribute to frequency control, since they are usually operated in a maximum power point tracking mode [4]. Moreover, varying weather conditions affect RES generation levels and, hence, the number of committed conventional generators is changing over time. Consequently, total inertia level, provided by rotating mass, and the damping of the system, provided by e.g. Power System Stabilizers (PSS) and damper windings, are varying in time. To ensure stable grid operation, the frequency control needs to be designed to perform well for a range of system conditions, where the system inertia and damping levels are uncertain. In control theory, an approach for designing controllers, explicitly dealing with uncertainty, is robust control.

G. S. Misyris, S. Chatzivasileiadis and T. Weckesser are with the Department of Electrical Engineering, Technical University of Denmark, 2800 Kgs. Lyngby, Denmark (e-mail: {gmisy, spchatz, jtgw}@elektro.dtu.dk).

978-1-5386-4505-5/18/$31.00

Several methods have been developed for enhancing stability under consideration of low system inertia and damping. The authors of [5]–[7] address the problem by proposing an optimization that informs system operators how to choose optimal levels of inertia with respect to damping of power system oscillations, while ensuring admissible transient behavior after a large disturbance. In [8], the authors propose an explicit model predictive control, which allows to directly incorporate operational constraints of power system units (ramp-rate, power rating, energy constraints) to achieve real-time tractability while keeping the online computation effort low. In [9], the authors propose an extended control loop based on the generator emulation control concept to provide inertia by using the stored energy in the dc-link capacitors of VSC-HVDC links. Moreover, researchers have been seeking different ways to control power electronic converters in power systems to enhance system stability [10]. One approach is to embed the dynamics and behavior of conventional synchronous machines into power electronic converters as Virtual Synchronous Machines (VSMs) [11], [12].

To implement this approach structured controllers are added to the control circuits of the converters. Structured controllers, such as PID, lead-lag controllers, etc. are preferred due to their properties, since they are easy to implement and re-tune whenever performance or system properties change. However, the uncertain RES power infeed makes the tuning procedure of the controllers challenging. Several methods have been proposed to increase robustness of structured controllers [13]. Among those methods, the H_∞ loop shaping methodology introduced in [14] is a good technique for combining desirable properties such as tracking performance, disturbance rejection, robustness to model uncertainty.

This paper first investigates the impact of time-varying inertia and damping on the frequency dynamics of the system. An analysis is conducted using tools from control system theory on how the uncertainty of those parameters affect frequency dynamics. Then, a structured robust control design is proposed to increase the security of the system operation under uncertainty. Reducing ROCOF and maximum frequency deviation is associated with inertia response and primary frequency control [8]. Most existing converter and generation systems use proportional control – in the form of droop control – to stabilize frequency right after a disturbance. Therefore, in this paper the focus is on proportional control for the robust control design. In the analysis, the frequency dynamics are represented by a second order model.

Accounting for the uncertainty of system dynamics due to the fluctuation of system inertia, the contribution of this paper is to propose a procedure for designing Multi-Input-Multi-Output (MIMO) controllers by exploiting the efficiency of the H_∞ loop shaping in synthesizing optimal and robust structured controllers. The outcome of the proposed design will be a state feedback controller that improves the power oscillation damping and decreases the ROCOF and the frequency overshoot for a wide range of system inertia and damping levels.

This paper is organized as follows: Section II describes the power system model considered in the control design procedure. Section III presents an analysis of the impact of varying inertia on the frequency dynamics of the power system. Section IV presents the procedure for deriving the robust controller. Section V demonstrates robust performance of the implemented controller. Conclusions are drawn in Section VI.

II. Power System Modeling

A. Dynamic generator model

A commonly used model to assess dynamic phenomena in power systems is the swing equation, see Eq. (1). It relates the change of rotor speed of a machine i to a torque imbalance.

$$\Delta\dot{\omega}_i = \frac{1}{2H_i}[\Delta T_{m_i} - \Delta T_{e_i}], \tag{1}$$

$$\Delta\dot{\delta}_i = \omega_0 \Delta\omega_{\mathrm{i}}, \tag{2}$$

where i refers to the number of the bus, $\Delta\omega_i$ is the per unit speed deviation, H_i is the inertia constant of the machine $[\frac{\mathrm{MW\cdot s}}{\mathrm{MVA}}]$, ΔT_{e_i} is the electrical torque deviation [p.u.] and ΔT_{m_i} is the deviation of the mechanical torque applied to the machine [p.u.]. $\Delta\delta_i$ is the rotor angle deviation in electrical radians and ω_0 is the base rotor electrical speed in radians per second. (1) and (2) formulate the equations of motion linearized around an operating point.

The change in electrical torque (ΔT_{e_i}) following a disturbance can be resolved into two components, the synchronizing torque component (ΔT_{S_i}) and the damping component (ΔT_{D_i}). (3) describes this change [2]:

$$\Delta T_{e_i} = \Delta T_{S_i} + \Delta T_{D_i} = K_{S_i}\Delta\delta_i + K_{D_i}\Delta\omega_i, \tag{3}$$

where ΔT_{S_i} is in phase with $\Delta\delta_i$, and K_{S_i} is the synchronizing torque coefficient; and ΔT_{D_i} is in phase with $\Delta\omega_i$, and K_{D_i} is the damping torque coefficient. Synchronizing torque depicts the non-linear nature of dynamics of interconnected generators. Insufficient synchronizing torque can lead to transient instability. On the other hand, lack of sufficient damping torque leads to oscillatory instability.

Although the swing equation is a simplified representation of power system dynamics, it can model adequately well first swing instability [2], [15]. Since the goal of this paper is to limit the maximum ROCOF and maximum frequency deviation, which usually appear during the first swing, the swing equation can represent sufficiently well the generator dynamics. Beside that, this modeling approach has been widely used in literature as a first step to gain insights and develop control approaches for a large number of power system stability problems.

In a "conventional" grid, synchronous generators ensure system stability, supported by Automatic Voltage Regulators (AVR) and PSS, which affect the magnitude of K_{S_i} and K_{D_i}. However, with high penetration of fluctuating RES, the number of committed synchronous generators vary, and with them the number of AVR and PSS, operating at each time instant. As a result, K_{S_i} and K_{D_i} vary with time. To counter the varying nature of K_{S_i} and K_{D_i}, new robust control approaches need to be developed.

B. State Space Model

Taking into consideration (1)-(3), the state space representation of the dynamics at each generator or aggregated generator unit is given by (4). This state space representation is of the form $\dot{x} = Ax + Bu$:

$$\underbrace{\begin{bmatrix}\Delta\dot{\omega}_{\mathrm{i}}\\ \Delta\dot{\delta}_{\mathrm{i}}\end{bmatrix}}_{\dot{x}_i} = \underbrace{\begin{bmatrix}-\frac{K_{D_i}}{2H_i} & -\frac{K_{S_i}}{2H_i}\\ \omega_0 & 0\end{bmatrix}}_{\mathrm{A_i}}\underbrace{\begin{bmatrix}\Delta\omega_{\mathrm{i}}\\ \Delta\delta_{\mathrm{i}}\end{bmatrix}}_{x_i} + \underbrace{\begin{bmatrix}\frac{1}{2H_i}\\ 0\end{bmatrix}}_{\mathrm{B_i}}\underbrace{\Delta T_{m_i}}_{u_i} \tag{4}$$

where x_i is a vector containing the system state variables, A_i is a matrix termed as the state matrix of the system, B_i is the input matrix and u_i contains the system input variables. The order of A_i matrix determines the number of modes of the system and the system eigenvalue properties.

The elements of the state matrix A_i are dependent on the system parameters K_{D_i}, K_{S_i}, H_i and the initial operating condition. The coefficients K_{S_i} and K_{D_i} can be calculated given an initial operating point based on (5) and (6), respectively.

$$K_{S_i} = \sum_{j\in\Omega_i} V_i V_j b_{ij} cos(\delta_{ij}) \tag{5}$$

$$K_{D_i} = \mathrm{c_{d_i}} \tag{6}$$

where V_i is the bus voltage magnitude, b_{ij} is the susceptance between i and j, δ_{ij} is the angle difference between i and j nodes, $\mathrm{c_{d_i}}$ is a constant value that represents the magnitude of the damping torque coefficient at each generator bus and Ω_{p} the set of all nodes adjacent to node p. Power losses are neglected.

C. Multi-machine system

In (4), $\Delta\omega_i$ represents the rotor speed. In a multi-machine system, the frequency measured at a particular bus is a function of the rotor speeds of all generators. In the following, it is assumed that larger regions of a power system are aggregated and represented by an equivalent machine. The dynamics of this equivalent machine can be described by (4) and the model parameters are determined through aggregation of the individual generators in the region. Consequently, the parameters H_i, K_{D_i} and K_{S_i} of the equivalent machine vary depending on the generation dispatch and power infeed of RES in the region. In the proposed modeling approach, the rotor speed dynamic response of the equivalent machine corresponds to the frequency dynamic response in the region. The overall aim is to develop a robust controller which improves the rotor speed

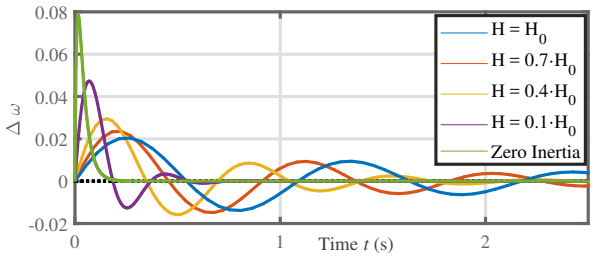

Fig. 1. $\Delta\omega$ impulse response at different inertia levels

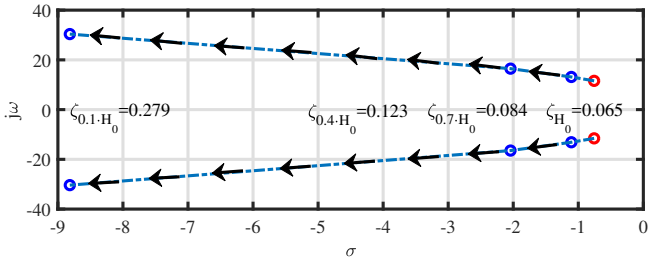

Fig. 2. Eigenvalues trajectory concerning the oscillatory mode of generator 3 (3-bus system, Section V), while reducing inertia level at bus 2 (ζ: Damping Ratio)

dynamic response of that equivalent machine, and, hence, the frequency response of the aggregated region. Therefore, in the rest of this paper, the terms rotor speed of the equivalent machine and frequency are used interchangeably.

For the observation of the frequency dynamics in multi-machine systems, the focus is on electromechanical oscillatory modes, which indicate how the generators oscillate against each other [2]. The second order model, defined by (4)-(6), can be used to describe the electromechanical oscillations of each generator. The multi-machine system is linearized over an equilibrium x_0, using Taylor approximation [2]. The connectivity between two buses i and j at an equilibrium, and the LaPlacian of the network, are given by:

$$P_{ij} = V_i V_j b_{ij} cos(\delta_{ij}), \qquad L_{ij} = \begin{cases} -P_{ij}, & i \neq j \\ K_{S_i}, & i = j \end{cases} \tag{7}$$

where K_{S_i} and P_{ij} are given by (5) and (7), respectively. Assuming a system with n buses, $\boldsymbol{L_N} \in R^{n\times n}$. The parameters of the system, such as inertia and damping, are collected in matrix form and the states in vectors.

$$\boldsymbol{H}_{\mathrm{N}} = \mathrm{diag}(2H_1, \cdots, 2H_{\mathrm{n}}),\ \boldsymbol{K}_{\mathrm{N}} = \mathrm{diag}(K_{D_1}, \cdots, K_{D_{\mathrm{n}}}) \tag{8}$$

$$\boldsymbol{\Delta\delta}_{\mathrm{N}} = [\Delta\delta_1, \cdots, \Delta\delta_n]^{\mathrm{T}}, \quad \boldsymbol{\Delta\omega}_{\mathrm{N}} = [\Delta\omega_1, \cdots, \Delta\omega_{\mathrm{n}}]^{\mathrm{T}} \tag{9}$$

where H_i is the inertia at each bus and K_{D_i} is given by (6), with $\boldsymbol{H}_{\mathrm{N}} \in R^{\mathrm{n}\times\mathrm{n}}$ and $\boldsymbol{K}_{\mathrm{N}} \in R^{\mathrm{n}\times\mathrm{n}}$. The state vectors $\boldsymbol{\Delta\delta}_{\mathrm{N}}$ and $\boldsymbol{\Delta\omega}_{\mathrm{N}}$ include the deviation of generators' rotor angles and speeds of the system, with $\boldsymbol{\Delta\delta}_{\mathrm{N}} \in R^{\mathrm{n}\times\mathrm{n}}$ and $\boldsymbol{\Delta\omega}_{\mathrm{N}} \in R^{\mathrm{n}\times\mathrm{n}}$.

The input for the multi-machine system is the vector containing the deviation of mechanical torque of each generator and the output is a vector containing the angular velocity deviation of each generator. The state space representation of the open-loop transfer function is:

$$\begin{cases} \dot{x} = \boldsymbol{A_{sys}} x + \boldsymbol{B_{sys}} u \\ y = \boldsymbol{C} x \end{cases} \tag{10}$$

$$\boldsymbol{A_{sys}} = \begin{bmatrix} \boldsymbol{O_{n\times n}} & \boldsymbol{\omega_{0_{n\times n}}} \\ -\boldsymbol{H_N^{-1}} \boldsymbol{L_N} & -\boldsymbol{H_N^{-1}} \boldsymbol{K_N} \end{bmatrix}, \ \boldsymbol{B_{sys}} = \begin{bmatrix} \boldsymbol{O_{n\times n}} \\ -\boldsymbol{H_N^{-1}} \end{bmatrix} \tag{11}$$

$$x = \begin{bmatrix} \boldsymbol{\Delta\delta_N} & \boldsymbol{\Delta\omega_N} \end{bmatrix}^{\mathrm{T}}, \qquad u = \begin{bmatrix} \Delta T_{m_1}, \cdots, \Delta T_{m_n} \end{bmatrix} \tag{12}$$

where x, A_{sys}, B_{sys} and u are given by (11) and (12). $\boldsymbol{O_{n\times n}}$ and $\boldsymbol{\omega_{0_{n\times n}}}$ are diagonal matrices, containing zero and ω_0 in their diagonal entries, respectively. C is a matrix mapping the speed deviation of each generator or generator unit ($\Delta\omega_{\mathrm{i}}$). The transfer function $G(s)$ of the open-loop system is:

$$G(\mathrm{s}) = \frac{Y(\mathrm{s})}{U(\mathrm{s})} = C(\mathrm{s}I - A_{sys})^{-1} B_{sys} \tag{13}$$

III. Analysis of Impact of Varying Inertia and Damping on Frequency Dynamics

A. Modal analysis

To quantify the effect of the varying system inertia and damping, modal analysis, Bode gain and eigenvalue plots are used to visualize the response of the examined system. For the presented case study the following assumptions are made:

1) The voltage dynamics and the dynamics for reactive power compensation are not included.
2) Under varying penetration of RES, the decrease rate of system inertia (H_{sys}) is higher than the one of system damping ($K_{D_{\mathrm{sys}}}$).

B. Sensitivity Analysis - Time varying parameters

For the sensitivity analysis, the inertia and damping parameters at generator bus 2 are varying. Similar results can be extracted by varying the parameters at other other generator buses. It is worth mentioning that, in the examined system (Fig. 8), there are two oscillatory modes, one associated with generators 1 and 3 and the other with generators 2 and 3.

Fig. 1 presents the impulse response of the frequency deviation at a system node, where an equivalent machine is connected. As it can be observed, the frequency overshoot and ROCOF greatly depends on inertia levels: the lower the inertia is, the higher the frequency deviation and ROCOF become. This could also be explained by (1), where decreasing system inertia results to higher rate of frequency deviation for the same magnitude of torque imbalance. Moreover, decrease of inertia levels leads to increased damping ratio. This can be seen both in Figs. 1 and 2, where the trajectory of the eigenvalues of electromechanical mode associated with generators 2 and 3 for a 90% reduction of inertia level are presented. As seen in Fig. 2, at the initial level of inertia the eigenvalues indicate low damping ratio (red circles). While decreasing the inertia level, the eigenvalues move further to the left, which results to higher damping ratio.

In Fig. 3 the Bode plot of $G_2(s) = \frac{\Delta\omega_2(s)}{\Delta T_{m_2}(s)}$ is illustrated. To evaluate the system response, the rise-time, the overshoot and the settling time parameters are used [16]. Considering $G_2(s)$, the system rise-time is associated with the ROCOF and the system overshoot with the maximum frequency deviation. As shown in the figure, reducing system inertia leads to gain amplification at higher frequencies and an increase of the system bandwidth (also illustrated in Fig. 4), which results

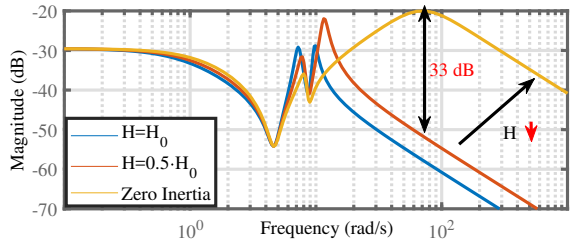

Fig. 3. Frequency Response of $G_2(s)$ for different levels of inertia. (H:Inertia)

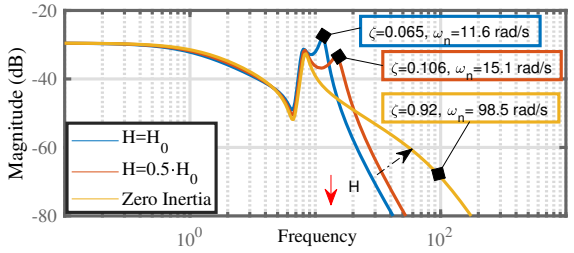

Fig. 4. Frequency Response of $G_{32}(s)$ for different levels of inertia. (H: Inertia, ζ: Damping ratio of the electromechanical modes, $omega_n$: Natural Frequency of the mode)

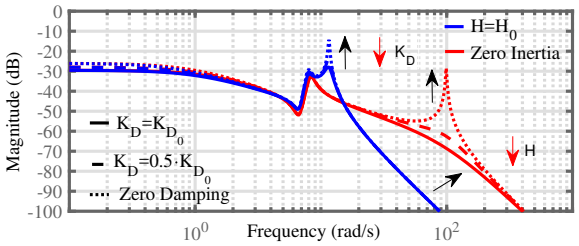

Fig. 5. Frequency response of $G_{32}(s)$ for different levels of damping and inertia. (K_D: Damping Torque Coefficient, H: Inertia)

to shorter rise-time and higher overshoot [16] (also illustrated in Fig. 1). In Fig. 4 the Bode plot of $G_{32}(s) = \frac{\Delta\omega_3(s)}{\Delta T_{m_2}(s)}$ is illustrated. As the inertia level decreases, the magnitude of the transfer function becomes smaller around the frequency of electromechanical modes (3.5-12 rad/s), which results to better damping of the oscillatory mode associated with generators 2 and 3. As for the oscillatory mode of generators 1 and 3, its damping ratio and frequency are insignificantly different, therefore in terms of brevity the results are not depicted.

Fig. 5 presents the frequency response for different levels of damping and inertia. Blue lines represent the case with high inertia and red lines the case with the low inertia. As the damping decreases, the gain becomes larger at the frequencies of oscillatory modes and the system becomes undamped [16]. Moreover, it can be seen that the varying inertia affects the frequency of the oscillatory modes. In particular, as inertia level becomes lower, the frequency of the oscillatory modes become higher. It is worth mentioning, however, that the steady state gain (below 1 rad/s) remains almost constant despite the varying inertia and damping.

Based on these observations, the goal in this paper is to derive a robust control approach to compensate the impact of damping and inertia (varying penetration of RES), while not altering the steady-state behavior of the system.

IV. Structured Robust Controller

A. H_∞ Loop shaping design

In [14] the authors proposed an H_∞ design procedure, in which the desired performance of the controller can be specified by shaping the singular values of the nominal system system $G(s)$ using pre- and post-compensators $W_1(s)$ and $W_2(s)$. The H_∞ design procedure is applied for a PID controller in [17], [18]. Since the focus is on tuning the gains of a structured proportional controller (P-controller), the above design procedure is adjusted. In this framework, the controller $K(s)$, see Fig. 6, is structured as:

$$K(s) = W_1(s)^{-1} K_{\mathrm{P}}(s) \tag{14}$$

where W_1 and W_1^{-1} are stable transfer matrices and K_{P} is the transfer matrix of the P-controller. The transfer matrix K_{P} is a diagonal matrix with the proportional gains as elements, which correspond to the gains of each P controller of every bus ($K_{\mathrm{P}} = \mathrm{diag}(k_{p_1}, k_{p_2} \cdots k_{p_n})$, where n is the number of buses considered in the system). This particular structure of Fig. 6 ensures that the final controller has the desired P-structure since K_{final}=$W_1 {W_1}^{-1} K_{\mathrm{P}} W_2$ = $K_{\mathrm{P}} W_2$ [17].

The input-output relationship of the closed-loop system, see Fig. 6 is given by:

$$\underbrace{\begin{bmatrix} z_1 \\ z_2 \end{bmatrix}}_{\mathbf{z}} = T_{zw}(K_{\mathrm{P}}) \underbrace{\begin{bmatrix} w_1 \\ w_2 \end{bmatrix}}_{\mathbf{w}} \tag{15}$$

$$T_{zw}(K_{\mathrm{P}}) = \begin{bmatrix} (I + W_2 G K_{\mathrm{P}})^{-1} W_2 G W_1 & (I + W_2 G K_{\mathrm{P}})^{-1} \\ -W_1^{-1} K_{\mathrm{P}} (I + W_2 G K_{\mathrm{P}})^{-1} W_2 G W_1 & -W_1^{-1} K_{\mathrm{P}} (I + W_2 G K_{\mathrm{P}})^{-1} \end{bmatrix}$$
$$= \begin{bmatrix} I \\ -W_1^{-1} K_{\mathrm{P}} \end{bmatrix} (I + W_2 G K_{\mathrm{P}})^{-1} \begin{bmatrix} W_2 G W_1 & I \end{bmatrix} \tag{16}$$

where $G(s)$ is the initial plant of the system. After determining $T_{zw}(K_{\mathrm{P}})$ the objective is to find the K controller that satisfies the following optimization problem:

$$\begin{aligned} &\text{minimize } \gamma \\ &\text{subject to } ||T_{zw}(K_{\mathrm{P}})||_\infty \leq \gamma \end{aligned} \tag{17}$$

After solving the optimization problem, described in (17), the final controller is given by:

$$K_{\mathrm{final}}(s) = K_{\mathrm{P}}(s) W_2(s) \tag{18}$$

which corresponds to a standard P controller in cascade with the post-compensator $W_2(s)$.

In the following subsection the procedure of deriving the weighting functions is presented. The minimal achievable value of $||T_{zw}(K_{\mathrm{P}})||_\infty$ indicates that the closed-loop system is bounded by a value of γ at all frequencies, which indicates the robust performance of the closed loop system (Fig. 6) against uncertainty. The values for the parameter γ range between 1 and 3 [13]. The closer to 1 is the value of γ the more robust is the performance of the closed loop system. In case $\gamma \geq 3$ the W_1 and W_2 have to be adjusted until the condition ($1 \leq \gamma \leq 3$) is satisfied [13].

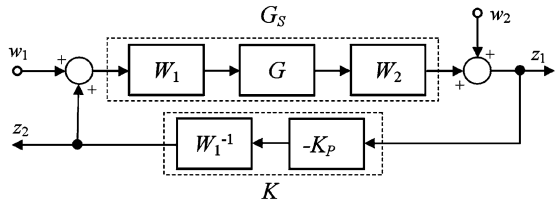

Fig. 6. Shaped Plant and Controller [19]

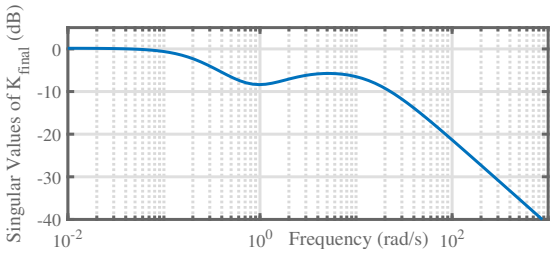

Fig. 7. Singular Values of controller K_{final}

B. Weighting Functions

According to [13] and Fig. 6, W_2 reflects the relative importance of the outputs to be controlled being fed back to controller and W_1 contains the dynamic shaping such as an integral action for low frequency performance and disturbance attenuation. By this means W_1 determines the gain at low and W_2 the gain at high frequencies.

The objective of the controller is determined based on the results presented in Section III. As mentioned above and depicted in Fig. 5, varying inertia affects the gain in the higher frequencies and varying damping the gain at the frequencies of electromechanical modes. Therefore, concerning the varying inertia, it is desirable that the robust controller exposes the characteristics of a low pass filter with a cut-off frequency in the range of 15-20 rad/s. As for the varying damping, to increase resilience to damping uncertainty, a bandstop filter is required at the frequencies of oscillatory modes (2-15 rad/s). Considering the above and the H_∞ design procedure [17], pre- and post- compensators are chosen accordingly.

The desired loop shape of the controller $K_{\text{final}}(s)$ is depicted in Fig. 7. The singular values [20] of the frequency response of the controller is depicted. The maximum singular value indicates the maximum amplification of the corresponding inputs by the system seen from a specific output. As it is illustrated, the controller has zero gain at low frequencies, which indicates the system is not affected within that range by the controller. At mid-range and higher frequencies, it can be seen that the controller results to a negative gain and consequently will increase the damping ratio and decrease ROCOF and maximum frequency deviation.

V. Results

A. 3-Bus System

To evaluate the robust control, the 3-Bus System presented in Fig. 8 is used. The state variables of the 3-Bus System are collected in vectors and in the form $\dot{\mathrm{x}} = \mathrm{A_{sys}x} + \mathrm{B_{sys}}u$,

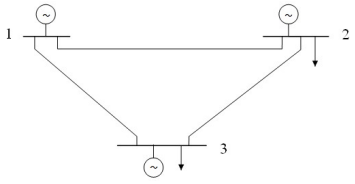

Fig. 8. 3-Bus System.

TABLE I
Bus voltages, Mechanical inputs, Static loads

Node	Voltage [p.u.]	Power [p.u.]	Damping K_{D_i}	Inertia H_i
1	1.0526	-1.5	10	5.5
2	1.0502	1.05	10	2.75
3	1.017	0.45	10	5.5

see (10). The system characteristics are given in Table I. The susceptances of the transmission lines are: $b_{12} = 0.739$, $b_{13} = 1.0958$ and $b_{23} = 1.245$. At the operating point, the synchronizing torque coefficients of the state space model can be calculated by (5). The values of the damping torque coefficients at each generator bus are given in Table I.

Having derived the state space model of the 3-Bus system and the transfer function for the actual plant $G(s)$ using (13), the robust control design technique, presented in Section IV, is implemented. Once the proportional controller is tuned and the state feedback gain is defined, then it is added to each bus of the 3-Bus system. There are 3 additional state variables in the second order model describing the frequency dynamics of each bus. Considering the two cases mentioned above, the results for the frequency deviation at bus 2 of the 3-Bus system are presented. The transfer function of the closed loop system with $\mathrm{K_{final}(s)}$ as a controller and a negative feedback gain is:

$$CL_{\text{sys}}(s) = \frac{G(s)K_{\text{final}}(s)}{1 + G(s)K_{\text{final}}(s)} \tag{19}$$

B. Case 1 - low inertia

In case 1 the performance and the response of the system after 50% reduction of the inertia level at bus 2 is evaluated. As illustrated in Fig. 9, low inertia results to higher frequency deviation and overshoot compared to the initial levels. The effect of the controller, applied during operation of the system with low inertia, results to smaller maximum frequency deviation and lower ROCOF. This can be explained by seeing Fig. 7, where it is depicted that the controller decreases the gain of the system transfer function at high frequencies. Overall, the results and the impact of the controller on system response are summarized in Table II, where the values of ROCOF, maximum frequency deviation and settling time are presented for this particular case.

C. Case 2 - low damping

In case 2 the performance and the response of the system after 60% reduction of the damping torque coefficient at bus 2 is evaluated. As shown in Fig. 10, lower K_D results to

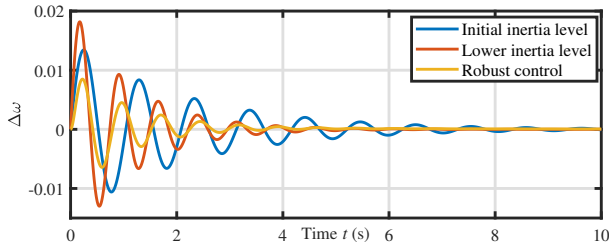

Fig. 9. Robust control of $\Delta\omega$ & impulse response for 50% reduction of the initial inertia level.

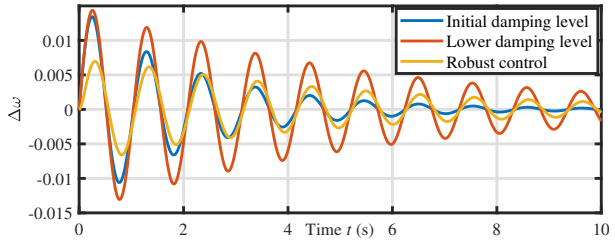

Fig. 10. Robust control of $\Delta\omega$ & impulse response for 60% reduction of the initial damping level.

shorter settling time and damping of the oscillations, and has no impact on frequency overshoot. The effect of the controller, applied during operation of the system with lower K_D, results to lower frequency deviation and ROCOF, and has a positive effect on damping of oscillations. However, it does not compensate for the 60% reduction of K_D, as it has longer settling time, see Fig. 10, compared to initial operation of the system. Thus, it does not increase the damping ratio significantly. The impact of the controller on system response for 60% reduction of the initial damping level is depicted in Table III.

VI. Conclusions & Future Work

In this paper, the impact of the time-varying inertia and damping on grid operation has been addressed using frequency domain analysis. The results showed that the varying inertia increases ROCOF and maximum frequency deviation, but improves damping. To compensate for the increased uncertainty caused by these time-varying parameters, a robust controller is implemented. The proposed controller deals with the negative effect of the varying inertia and damping on the frequency dynamics. Concluding, through the use of an H_∞ loop shaping design procedure, the developed controller increases the resilience of the system to imminent disturbances in the case of high penetration of RES.

Future work intends to evaluate the proposed methodology on higher order power system models and extend the robust control to large systems.

VII. Acknowledgement

This work is supported by the multiDC project, funded by Innovation Fund Denmark, Grant Agreement No. 6154-00020B.

TABLE II
Case 1 - low inertia

	ROCOF ($\frac{\text{pu}}{\text{s}}$)	Overshoot (pu)	Settling t (s)
Initial Inertia	0.0909	0.013	8.66
Lower Inertia	0.1817	0.018	4.31
Robust Control	0.0031	0.008	5.51

TABLE III
Case 2 - low damping

	ROCOF ($\frac{\text{pu}}{\text{s}}$)	Overshoot (pu)	Settling t (s)
Initial Damping	0.0909	0.013	8.66
Lower Damping	0.0909	0.013	21.60
Robust control	0.0016	0.006	17.52

References

[1] A. Ulbig, T. S. Borsche, and G. Andersson, "Impact of low rotational inertia on power system stability and operation," *IFAC Proc. Vol.*, vol. 47, no. 3, pp. 7290 – 7297, 2014, 19th IFAC World Congress.

[2] P. Kundur, N. Balu, and M. Lauby, *Power system stability and control*, ser. EPRI power system engineering series. McGraw-Hill, 1994.

[3] P. Tielens and D. V. Hertem, "The relevance of inertia in power systems," *Renew. Sust. Energ. Rev.*, vol. 55, pp. 999 – 1009, 2016.

[4] F. Wilches-Bernal, J. H. Chow, and J. J. Sanchez-Gasca, "A fundamental study of applying wind turbines for power system frequency control," *IEEE Trans. Power Syst.*, vol. 31, no. 2, pp. 1496–1505, Mar. 2016.

[5] T. S. Borsche, T. Liu, and D. J. Hill, "Effects of rotational inertia on power system damping and frequency transients," in *2015 54th IEEE Conference on Decision and Control (CDC)*, Dec. 2015, pp. 5940–5946.

[6] B. K. Poolla, S. Bolognani, and F. Dörfler, "Optimal placement of virtual inertia in power grids," *IEEE Trans. Autom. Control*, vol. 62, no. 12, pp. 6209–6220, Dec. 2017.

[7] D. Gross, S. Bolognani, B. Poolla, and F. Dörfler, "Increasing the Resilience of Low-inertia Power Systems by Virtual Inertia and Damping," in *IREP Bulk Power System Dynamics & Control Symposium*, Sep. 2017.

[8] A. Ulbig, T. Rinke, S. Chatzivasileiadis, and G. Andersson, "Predictive control for real-time frequency regulation and rotational inertia provision in power systems," in *52nd IEEE Conference on Decision and Control*, Dec. 2013, pp. 2946–2953.

[9] X. Liu and A. Lindemann, "Control of VSC-HVDC connected offshore windfarms for providing synthetic inertia," *IEEE Trans. Emerg. Sel. Topics Power Electron.*, vol. PP, no. 99, pp. 1–1, Sep. 2017.

[10] Q. C. Zhong, "Virtual synchronous machines: A unified interface for grid integration," *IEEE Power Electron. Mag.*, vol. 3, no. 4, pp. 18–27, Dec. 2016.

[11] H. P. Beck and R. Hesse, "Virtual synchronous machine," in *2007 9th International Conference on Electrical Power Quality and Utilisation*, Oct. 2007, pp. 1–6.

[12] Q. C. Zhong and G. Weiss, "Synchronverters: Inverters that mimic synchronous generators," *IEEE Trans. Ind. Electron.*, vol. 58, no. 4, pp. 1259–1267, Apr. 2011.

[13] S. Skogestad and I. Postlethwaite, *Multivariable Feedback Control: Analysis and Design*. John Wiley & Sons, 2005.

[14] D. McFarlane and K. Glover, "A loop-shaping design procedure using H_∞ synthesis," *IEEE Trans. Autom. Control*, vol. 37, no. 6, pp. 759–769, Jun. 1992.

[15] T. Weckesser and T. V. Cutsem, "Equivalent to represent inertial and primary frequency control effects of an external system," *IET Gener., Transm. & Dis.*, vol. 11, pp. 3467–3474(7), September 2017.

[16] G. C. Goodwin, S. F. Graebe, and M. E. Salgado, *Control System Design*. Prentice Hall, 2001.

[17] A. U. Genç and S. T. Impram, "A state-space algorithm for designing H_∞ loop shaping PID controllers," *IFAC Proc. Vol.*, vol. 36, no. 11, pp. 281 – 286, 2003, 4th IFAC Symposium on Robust Control Design 2003, Milan, Italy, 25-27 Jun. 2003.

[18] P. Apkarian, V. Bompart, and D. Noll, "Non-smooth structured control design with application to PID loop-shaping of a process," *Int. J. Robust Nonlin. Control*, vol. 17, no. 14, pp. 1320–1342, Jan. 2007.

[19] R. Toscano, *H 2 and Mixed H 2/H Design of Structured Controllers*. London: Springer London, 2013, pp. 199–231.

[20] K. Zhou and J. Doyle, *Essentials of Robust Control*, ser. Prentice Hall Modular Series for Eng. Prentice Hall, 1998.